Journal of Biomolecular NMR, **20:** 149–165, 2001.
KLUWER/ESCOM

An improved method for distinguishing between anisotropic tumbling and chemical exchange in analysis of ^{15}N relaxation parameters

Norma H. Pawley[a], Chunyu Wang[a], Shohei Koide[b] & Linda K. Nicholson[a,*]
[a]*Department of Molecular Biology and Genetics, 239 Biotechnology Building, Cornell University, Ithaca, NY 14853, U.S.A.*
[b]*Department of Biochemistry and Biophysics, University of Rochester Medical Center, Rochester, NY 14642, U.S.A.*

Received 5 January 2001; Accepted 16 April 2001

Key words: anisotropy, chemical exchange, dynamics, global tumbling

Abstract

Although an accurate description of global tumbling of a protein is essential for correct analysis of internal motions, proper distinction between the effects of anisotropic rotational diffusion and conformational exchange has remained a challenge. We present a novel two-part filtering procedure designed specifically to distinguish between the effects of anisotropy and conformational exchange. The efficacy of this method is assessed using synthetic data sets. The method is then applied to two proteins of dramatically different size and shape, OspA and SH3. The large size and extreme anisotropy of OspA provide a challenging case, where conformational exchange is a small perturbation of the effects of anisotropy on transverse relaxation rates. Conversely, in the chicken c-Src SH3 domain, with its small size and nearly spherical shape, anisotropy is a small perturbation of the effects of conformational exchange on transverse relaxation rates. Accurate extraction of the global tumbling parameters for each protein allows optimal characterization of conformational exchange processes, as well as ps–ns time scale motions.

Abbreviations: NOE, nuclear Overhauser effect; SH3, Src homology domain 3; OspA, Outer surface protein A; exp, experimental; calc, calculated; NORMAdyn, NMR Optimized Relaxation Modeling with Anisotropy, for dynamics analysis; CPMG, Carr-Purcell-Meiboom-Gill pulse sequence.

Introduction

^{15}N spin relaxation parameters have been widely used to characterize the motions of individual backbone N-H bonds within proteins, and have provided a powerful tool for probing the internal dynamics of proteins. The ^{15}N spin relaxation parameters (T_1, T_2, $T_{1\rho}$ and NOE) contain information on both the global and internal motions of N-H bond vectors. Hence, proper evaluation of site-specific internal motions relies upon an accurate description of the rigid body global tumbling of the protein. It has been widely recognized that correct characterization of global tumbling is hampered by the difficulty in distinguishing between the effects of anisotropy and conformational exchange on measured transverse relaxation rates (Schurr et al., 1994; Tjandra et al., 1995; Mandel et al., 1996; Kroenke et al., 1998; Andrec et al., 1999; de Alba et al., 1999).

Conformational exchange can be independently identified by measuring the dependence of the relaxation times on the static magnetic field strength (Phan et al., 1996), by rotating frame spin relaxation measurements (Akke and Palmer, 1996) or by transverse and longitudinal cross-correlation measurements (Kroenke et al., 1998). Since, however, these measurements require additional experimental resources (e.g., spectrometer time, deuterium labeling), initial investigations are often performed using only T_1, T_2 (or equivalently, $T_{1\rho}$) and NOE at a single field strength. Since these initial investigations are often used to motivate the application of other methods, the accurate distinction between the effects of anisotropy and con-

*To whom correspondence should be addressed. E-mail: lkn2@cornell.edu

formational exchange on transverse relaxation rates remains an important challenge.

The standard approach to global tumbling analysis using ^{15}N spin relaxation parameters is to use a subset of transverse and longitudinal relaxation times (T_1 and T_2) to obtain the rotational diffusion parameters that best fit the data. In the absence of significant internal motion, all measured T_1 and T_2 values could be used for determining the parameters that describe global tumbling of the molecule. However, when appreciable internal motions are present, the effects of these motions must be carefully separated from the effects of global tumbling (Schurr et al., 1994). More than one method has been proposed to address the separation of internal and global motions for accurate characterization of anisotropic tumbling. For auto-relaxation data collected at a single field strength, a common method for identifying and excluding residues with large-amplitude motions on the ps–ns time scale or affected by conformational exchange on the μs–ms time scale is that of Tjandra et al. (1995), hereafter referred to as the 'standard filter'. As recently pointed out, this method can falsely identify residues affected by anisotropic tumbling as residues experiencing conformational exchange (Andrec et al., 1999; de Alba et al., 1999). Removal of these residues from the data set used to fit the global tumbling can skew the results toward a more isotropic fit, since they hold the most information regarding the effects of anisotropic diffusion (Kroenke et al., 1998). Hence, a critical aspect of separation of global and internal motions is the ability to distinguish between the effects of anisotropy and chemical exchange.

In this paper we propose an alternate method that takes advantage of the correlated changes in T_1 and T_2 induced by anisotropic tumbling. Effective separation of anisotropic tumbling from internal motions is accomplished in a two-part process in which residues with significant internal motions are removed from the global tumbling analysis without eliminating residues that contain critical information regarding anisotropic tumbling. The proposed procedure also ensures that the fit of site-specific internal motions is not underdetermined. A comparison of experimental T_2 and $T_{1\rho}$ values is used to guard against bias from systematic errors in either parameter.

The efficacy of the proposed method is demonstrated by application to synthetic data sets, generated to simulate proteins with varying degrees of axially symmetric anisotropy, from nearly isotropic to significantly anisotropic. Performance of the proposed method is also compared to that of the standard filter. The method is then demonstrated on experimental data obtained for two proteins of different size and extent of anisotropy, OspA (Outer surface protein A) and SH3 (the SH3 domain of $pp60^{c-Src}$). OspA is a large (28 kDa), highly anisotropic protein that is a major surface antigen of the Lyme disease spirochete, *Borrelia burgdorferi*. The high-resolution (1.8 Å) structure of OspA has been solved by X-ray crystallography (Li et al., 1997), and NMR and small-angle X-ray scattering analyses have shown that the solution conformation of free OspA is similar to the crystal structure (Bu et al., 1998; Pham and Koide, 1998). For a protein the size of OspA, the rate of decay of transverse magnetization ($R_2=1/T_2$) is rapid. For axially symmetric anisotropic diffusion, R_2 varies with the angle (α) between the N-H bond and the unique axis of the diffusion tensor, $R_2(\alpha)$. Consequently, the influence of conformational exchange (manifested as a relaxation rate, R_{ex}) on the measured rate of transverse magnetization decay is particularly difficult to characterize, since it is typically a small fraction of the measured decay rate ($R_2(\alpha) + R_{ex}$). The SH3 domain derived from the non-receptor tyrosine kinase $pp60^{c-Src}$ is a small (8.4 kDa), relatively spherical domain that plays important regulatory roles in intracellular signal transduction. The SH3 structure has been extensively studied and measurement of hydrogen bonds in solution (Cordier et al., 2000) shows remarkable agreement with the 1.5 Å resolution X-ray structure of nearly intact Src (Xu et al., 1999). For proteins the size of SH3 that have small anisotropy, R_2 is smaller and varies only slightly with α. Hence, the influence of R_{ex} on the measured transverse relaxation rate is more pronounced, since R_{ex} is independent of the global tumbling rate and hence of molecular size. In this case, anisotropic tumbling is more difficult to distinguish, and can be misinterpreted in terms of internal motions. Therefore, it is of critical importance for both large and small proteins to clearly distinguish between the effects of chemical exchange and anisotropy on transverse relaxation rates in order to correctly interpret global and internal motions.

Materials and methods

Preparation of OspA NMR sample

The ^{15}N-enriched OspA NMR sample was prepared as described previously (Pham and Koide, 1998), and was composed of a 1 mM solution of ^{15}N-

labeled OspA in sodium phosphate buffer (10 mM, pH 6.0 at room temperature) containing sodium chloride (50 mM), EDTA (50 μM) and sodium azide (0.02%) in 95% H_2O/5% D_2O.

NMR experiments and data processing

NMR experiments on OspA were performed at 45 °C on a Varian Unity INOVA 600 spectrometer using a 5 mm self-shielded triple resonance probe with a z-axis pulsed field gradient. The temperature in the sample region of the probe was calibrated using a 100% methanol sample and verified using a 100% ethylene glycol sample (Raiford et al., 1979). NMR experiments on chicken c-Src SH3 at 25 °C will be described elsewhere (Wang, C. et al., unpublished results).

Backbone amide ^{1}H-^{15}N NOE and ^{15}N T_1, $T_{1\rho}$, and T_2 (CPMG) values were measured for OspA using published procedures (Farrow et al., 1994; Yamazaki et al., 1994). The T_1 relaxation decay was sampled at 9 different time points (0.0110, 0.0220, 0.0550, 0.110, 0.220, 0.385, 0.550, 0.826, and 1.10 s), with duplicate spectra recorded at 0.011 and 0.110 s. The $T_{1\rho}$ decay was sampled at 8 different time points (0.008, 0.016, 0.024, 0.032, 0.040, 0.056, 0.072, and 0.096 s), with duplicate spectra recorded at 0.008, 0.072, and 0.096 s. A ^{15}N spin-lock field strength of 2.3 kHz was used for the $T_{1\rho}$ measurements. The T_2 decay was sampled at 9 different time points (0.0165, 0.0331, 0.0496, 0.0662, 0.0827, 0.0993, 0.116, 0.149, and 0.182 s), with duplicate spectra recorded at 0.0165 and 0.0662 s. The interpulse delay between ^{15}N 180° pulses in the CPMG sequence was 0.9 ms. All experiments were performed using spectral widths of 2.13 × 9.00 kHz in the $t_1 \times t_2$ dimensions. T_1 and T_2 measurements used a recycle delay of 1 s; $T_{1\rho}$ measurements used a recycle delay of 2.5 s; NOE measurements used a recycle delay of 4.6 s. T_1, $T_{1\rho}$, and T_2 experiments were performed using a total of 16 transients per t_1 experiment, NOE experiments were performed using 32 transients. For T_1, T_2, and NOE, 400 × 1024 complex points were acquired in the $t_1 \times t_2$ dimensions. For $T_{1\rho}$, 360 × 1024 complex points were acquired. Resonance assignments for OspA have been previously reported (Pham and Koide, 1998). NMR data were processed using NMRPipe.

Analysis of ^{15}N relaxation data

Backbone amide ^{15}N T_1, $T_{1\rho}$, and T_2 relaxation times were determined by fitting of peak volumes as a function of relaxation decay time to a single-exponential decay function using conjugate gradient minimization (Nicholson et al., 1992). Peak volumes were obtained using nonlinear least squares analysis of peak lineshapes as implemented by nlinLS (Frank Delaglio, NIH/NIDDK). Uncertainties associated with T_1, $T_{1\rho}$, and T_2 values were estimated by Monte Carlo simulation as described elsewhere (Nicholson et al., 1992). Steady-state NOE values were determined from the ratio of the peak intensities with and without proton saturation (Grzesiek and Bax, 1993). Uncertainties in peak height measurements were estimated from noise in the baseplane, and uncertainties in NOE values were obtained by propagation of errors (Nicholson et al., 1992).

Data filtering

A new procedure is proposed for filtering out residues for which internal motions, in particular conformational exchange, significantly affect the measured relaxation parameters. The novel aspect of this method is in the first part of the filtering process, in which a coarse data filter is applied to the set of relaxation parameters obtained for the protein. As described below, the unique criterion of this filter optimizes retention of residues that hold important information regarding anisotropic tumbling. For a prolate ellipsoid these are the residues for which the N-H bond lies close to the unique axis of the diffusion tensor. The motivation for each filtering step is discussed below, in the order in which it is applied. The total filtering process requires the following steps:

Part one: Coarse filter

(1a) Residues with NOE < 0.65 are removed from the data set.

(1b) Residues with low values of T_2 $\left(T_2 \leq \langle T_2 \rangle - \sigma_{T_2}\right)$ are removed from the data set, unless their corresponding T_1 values are high $\left(T_1 \geq \langle T_1 \rangle + \sigma_{T_1}\right)$, indicating that they may be affected by anisotropic tumbling (vide infra).

Part two: Fine filter

(2a) An initial estimate of the global tumbling is determined, using residues surviving the coarse filter.

(2b) All residues are evaluated for the quality of fit to the Lipari–Szabo model of internal motion (Lipari and Szabo, 1982), using the initial estimate of global tumbling from step 2a. Residues that do not fit the Lipari–Szabo model (vide infra) are removed from the global tumbling data set. In addition, residues for which $\tau_f \geq 600$ ps are removed from the data set since these residues are likely to violate the fast internal motion assumption necessary for use of the

T_1/T_2 ratio in determination of the global tumbling and would not necessarily be removed by the NOE filter (step 1a). The remaining residues are used to calculate the optimal global tumbling parameters.

For a protein the size of OspA, the first step (1a) eliminates flexible residues. For example, residues for which $S^2 \cong 0.7$ that undergo motions on a time scale between $\sim$ 20 ps and 2 ns are eliminated. For residues for which $S^2 \cong 0.90$, the corresponding time range eliminated is between $\sim$ 70 ps and 1 ns. It should be noted that for residues undergoing motion on a time scale close to the proton T_1 minimum (ca. 300 ps), the NOE values are dramatically reduced. Specifically, the NOE cutoff of 0.65 will eliminate residues with S^2 as large as 0.95, but for a more narrow range of time scales ($\sim$230–370 ps for OspA). As indicated, the range of time scales eliminated becomes increasingly broad as S^2 decreases. Assuming a typical distribution of time scales of internal motion, the bulk of the residues removed in larger proteins will be those that experience large-amplitude motions. However, for a protein the size of SH3, the corresponding time scale range in which NOE $<$ 0.65 is $\sim$ 30 ps–1.9 ns for $S^2 \cong 0.7$, and $\sim$ 150–600 ps for $S^2 \cong 0.90$. For a protein the size of SH3 with $S^2 \cong 0.95$, no residues have NOE values that fall below the NOE $<$ 0.65 cutoff. Therefore, extremely rigid residues or residues experiencing either very fast or very slow motions will be retained. Hence, although the NOE cutoff value of 0.65 is commonly used, it has different effects for each protein, with a more narrow range of time scales eliminated for smaller proteins.

The cutoff value of 0.65 is used here for consistency with the standard filtering approach. This value could be adjusted for an individual protein based on an estimate of the isotropic global tumbling time from, for example, Stokes' Law (Cavanagh et al., 1996). In addition, a second NOE filtering step could be introduced following filter step 2a, using the coarse estimate of the global tumbling time to determine an appropriate NOE cutoff value.

The coarse filter, in particular step 1b, is designed to separate the effects of anisotropic tumbling from the effects of internal motion. The basis for the design of step 1b is summarized in Table 1. This filtering step is based on the fact that, although both anisotropic tumbling and internal motions can cause T_1 and T_2 to deviate from the average across the protein, the relative directions of the changes are indicative of their source. When the source is anisotropic tumbling, T_1 and T_2 can be either higher or lower than the average across the protein (Figure 1a,b), depending on the angle (α) between the N-H bond vector and the unique axis of the diffusion tensor (Figure 1c). For a prolate ellipsoid, T_1 will be higher and T_2 will be lower if α is less than the magic angle, 54.7°, reflecting the larger effective correlation time experienced by N-H bonds with larger projections along the unique axis of diffusion (Figure 1d). Similarly, T_1 will be lower and T_2 will be higher if α is greater than 54.7°, reflecting the smaller effective correlation time experienced by N-H bonds perpendicular to the unique axis of diffusion. Hence, anisotropic tumbling causes T_1 and T_2 to shift in opposite directions from each other in a correlated manner (Figure 1d). The effects on T_1 and T_2 are reversed for an oblate ellipsoid (Table 1). For internal motion on the ps–ns time scale, the direction of the expected changes in T_1 and T_2 can be predicted based on the heteronuclear NOE, as illustrated in Table 1. For internal motion on the μs–ms time scale, T_2 may be lower than average, while T_1 is unaffected by these motions.

Step 1b of the filter is applied by calculating the average $<T_i>$ and standard deviation (σ_{T_i}) of the T_i (i=1,2) values across the protein. Residues with a low value of T_2 $\left(T_2 \leq \langle T_2 \rangle - \sigma_{T_2}\right)$ are cut, unless they have a corresponding high value of T_1 $\left(T_1 \geqslant \langle T_1 \rangle + \sigma_{T_1}\right)$. Using this criterion, residues with a low value of T_2 due to anisotropic tumbling are preserved, while residues with a low value of T_2 due to a significant contribution from chemical exchange are excluded.

Part two of the filtering process, the fine filter, requires that an initial estimate of the global tumbling be determined. This initial estimate is carried out in step 2a. This step requires knowledge of the orientation of the N-H bond vectors with respect to an arbitrary reference frame. For the synthetic data sets, N-H bond vector orientations were generated as described below. For the experimental data, the orientations were extracted with respect to the moment of inertia tensor for the respective structures of OspA (Li et al., 1997) and SH3 (Xu et al., 1999). The moment of inertia tensor was calculated using standard procedures, and the orientation of this tensor relative to the molecular frame was used as a starting point in fitting global tumbling parameters to the data.

The global tumbling parameters for the data surviving the coarse filter were determined by minimizing the error-weighted difference between the experimental and calculated T_1/T_2 ratios, χ_g^2 (Palmer et al.,

Table 1. Deviations in measured ^{15}N relaxation parameters from their average values as a result of N-H bond vector orientation or internal motion, and criteria of the coarse filter

	Anisotropic tumbling				Coarse filter[a]	Internal motion		Internal
	Prolate		Oblate		NOE ≤0.65	ps–ns		motion
	$\alpha < 54.7°$	$\alpha > 54.7°$	$\alpha < 54.7°$	$\alpha > 54.7°$		NOE ≤ 0.65	NOE ≥ 0.75	μs–ms
T_1	higher	lower	lower	higher	same or lower	higher	lower	same
T_2	lower	higher	higher	lower	lower	higher	lower	lower

[a]Residues are cut by the coarse filter if NOE < 0.65 or if both T_1 and T_2 deviate by more than one standard deviation from their average values as shown in the coarse filter column. This effectively separates residues affected by anisotropic tumbling from residues affected by internal motion on either the ps–ns or μs–ms time scales.

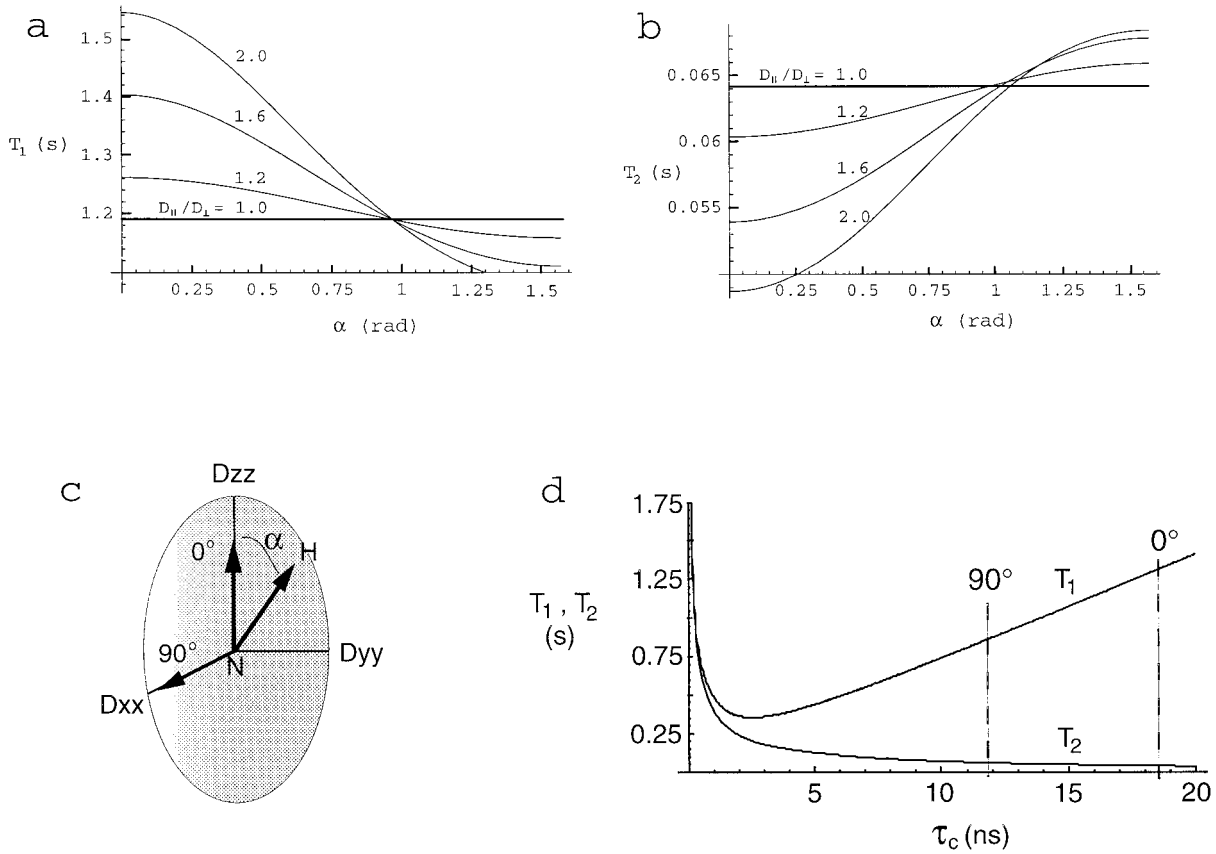

Figure 1. Effect of anisotropy on T_1 and T_2 for prolate ellipsoids. (a) T_1 as a function of α, for four values of $D_\parallel/D_\perp$. (b) T_2 as a function of α, for four values of $D_\parallel/D_\perp$. For a sin(α) probability distribution of N-H bond orientations, the average value of T_1 or T_2 corresponds to the average value of $\alpha \simeq 1$ rad (57.3°). Therefore, for proteins with a spherical distribution of N-H bonds, the average value of T_1 or T_2 will be very similar to the value for residues at the magic angle (54.7°), which is also very similar to the value for isotropic tumbling ($D_\parallel/D_\perp = 1$). Note that the effect of anisotropic tumbling is more readily apparent in the T_1 and T_2 values of residues with $\alpha \approx 0°$ than in residues with $\alpha \approx 90°$. (c) Ellipsoid corresponding to a prolate diffusion tensor showing three possible orientations of an N-H bond vector: along the principal axis of diffusion ($\alpha = 0°$), perpendicular to the principal axis of diffusion ($\alpha = 90°$), and at an arbitrary angle from the principal axis of diffusion. (d) T_1 and T_2 as a function of τ_c, for isotropic global tumbling ($S^2 = 1$). The vertical lines show that the values of T_1 and T_2 for residues with $\alpha = 0°$ and $\alpha = 90°$ in a protein with $D_\parallel/D_\perp = 2.1$, $\tau_c = 13.7$, are significantly different, reflecting the large difference in effective correlation time experienced by these N-H bonds.

1991):

$$\chi_g^2 = \sum_{i=1}^{N} \frac{\left(\left(\frac{T1_i}{T2_i}\right)_{\exp} - \left(\frac{T1_i}{T2_i}\right)_{calc}\right)^2}{\sigma_i^2}$$

where σ_i is the error in T_{1i}/T_{2i} obtained by propagation of errors (Nicholson et al., 1992) for residue i, and N is the number of residues used in the analysis. The theoretical T_1/T_2 ratio was calculated from standard analytical equations (Kay et al., 1989), using the form of the spectral density function for anisotropic global tumbling given by Woessner (1962). The value of χ_g^2 was calculated for each of three global tumbling models: isotropic, axially symmetric anisotropic, and fully anisotropic. The fully anisotropic model is described using six parameters: the principal axes of the diffusion tensor (D_{xx}, D_{yy} and D_{zz}), and the Euler angles (ϕ, θ and ψ) describing the rotational transformation from the inertia frame to the diffusion frame. For the axially symmetric model, $D_{xx} = D_{yy}$, and only θ and ϕ are required to describe the rotation. For the isotropic model, $D_{xx} = D_{yy} = D_{zz}$, and no rotation is required, since no orientation is preferred.

For efficiency in searching parameter space, a simulated annealing approach was employed, using χ_g^2 as the potential function. Once the minima were identified, the best minimum was 'polished' using a combination of conjugate gradient minimization for the principal axes of the diffusion tensor, and a grid search over the angular parameters. After the minimum χ_g^2 was determined for each model (isotropic, axially symmetric anisotropic, and fully anisotropic), the appropriate model was selected using the statistical F-test to determine the significance of the differences in χ_g^2:

$$F = \frac{(\chi^2_{g(N-m)} - \chi^2_{g(N-n)})(N-n)}{(n-m)\chi^2_{g(N-n)}}$$

where N is the number of data points, m is the number of fitted parameters in the first model, and n is the number of fitted parameters in the second model (n > m). Large values of F justify inclusion of additional terms in the fit. The probability that the improvement in the fit is obtained by chance when going from one model to a more elaborate model is given by P(F; n − m, N − n) (Bevington and Robinson, 1992). Values of $P < 0.01$ are typically considered highly significant (Taylor, 1982; Tjandra et al., 1996).

Filter step 2b is necessary for four reasons. First, it allows detection of residues affected by internal motion whose relaxation times did not fall outside of one standard deviation. Second, it enables identification of residues for which T_2 is raised by anisotropy, but lowered by chemical exchange, and that were therefore not detected by the coarse filter. Third, it detects residues with ns internal motions. These residues may cause T_1/T_2 to deviate significantly from the value at the extreme narrowing limit ($\tau_f \to 0$). Depending on the values of S^2 and τ_c, the time scale of motions that will not be detected by the NOE filter varies greatly. For $\tau_c = 5.9$ ns and $S^2 = 0.9$, the value of τ_f above which the NOE exceeds the 0.65 cutoff value is ~ 600 ps. As S^2 decreases and τ_c increases, the value of τ_f above which the NOE exceeds the 0.65 cutoff value increases. Hence, 600 ps should serve as a conservative general cutoff value. Finally, step 2b deals with the issue of underdetermined fitting. We define a residue as underdetermined if it requires a three-parameter model to fit the internal motions, and is also used to fit the global tumbling parameters. Therefore, in step 2b, any residues requiring three parameters to describe their internal motion are removed from the global tumbling data set.

To apply step 2b, the relaxation data (T_1, T_2, and NOE) for each residue are fit using the estimated global tumbling parameters from step 2a and the two site-specific parameters of the 'simple' Lipari–Szabo formalism (vide infra) by minimizing χ^2 for each residue:

$$\chi^2 = \frac{\left(T_1^{\exp} - T_1^{\text{calc}}\right)^2}{\sigma_{T_1}^2} + \frac{\left(T_2^{\exp} - T_2^{\text{calc}}\right)^2}{\sigma_{T_2}^2} + \frac{\left(NOE^{\exp} - NOE^{\text{calc}}\right)^2}{\sigma_{NOE}^2}$$

where the superscripts exp and calc denote the experimental and calculated values of T_1, T_2, and NOE, respectively. Residues for which χ^2 indicates a poor fit to the model ($\chi^2 = 6.8$, corresponding to the 99% confidence limit) and residues with internal motions on a time scale greater than 600 ps are then excluded from the data set, and the global tumbling parameters are fit to the new, more restricted, data set. This yields the final, best fit, global tumbling parameters. Similar iterative approaches have been used by others (Lee et al., 1997; Jia et al., 1999). Since three independent data are measured for each residue, and only those sites that are well described by a two-parameter model of internal motion are used to determine the global tumbling, the general problem of underdetermined fits is avoided (Andrec et al., 1999).

Analysis of parameters of motion

After the global tumbling parameters have been determined using the subset of the data that survived the total filtering process, the parameters of internal motion may be calculated for all residues in the protein, using the spectral density function for anisotropic rotational diffusion (Tjandra et al., 1996; Lee et al., 1997). The calculated values are obtained by using three different models for internal motion: (1) the two-parameter (S^2, τ_f) spectral density function (Lipari and Szabo, 1982); (2) the two-parameter spectral density function and an additional parameter to describe chemical exchange and other processes that contribute to the decay of transverse magnetization, (S^2, τ_f, R_{ex}) (Farrar and Becker, 1971); and (3) a three-parameter (S_f^2, S_s^2, τ_s) spectral density function (Clore et al., 1990). Three-parameter models were invoked only if the two-parameter model exceeded the 0.01 critical value of the incomplete gamma function ($\chi^2 > 6.8$), and if the three-parameter model could be fit with $\chi^2 = 0$ (Mandel et al., 1995; Nicholson et al., 1995). All of the analysis, starting from values of T_1, T_2 and NOE and ending with internal motion parameters, was performed using a suite of programs collectively referred to as NORMAdyn (NMR Optimized Relaxation Modeling with Anisotropy, for dynamics analysis) (N.H.P. and L.K.N., Cornell University).

Construction of synthetic data sets

To assess the accuracy and reliability of the filter, its performance was tested against synthetic data sets. The sets were constructed to fit axially symmetric anisotropic global tumbling, with two possible correlation times, $\tau_c = 5.92$ ns, and $\tau_c = 13.7$ ns, and three possible degrees of anisotropy, $D_\parallel/D_\perp = 1.2$, 1.6, and 2.0. The spectrometer field strength was set to 600 MHz. The angles (α) of the individual N-H bond vectors relative to the unique axis of the diffusion tensor, and values of S^2, τ_f and R_{ex}, were randomly drawn from the following distribution functions:

$$
\begin{aligned}
P(\alpha) &= \sin(\alpha) \cdot \{H(\alpha) - H(\alpha - \pi/2)\}/\Gamma_1 \\
P(S^2) &= e^{-(s^2 - s_0^2)^2/2\sigma_S^2} \cdot \{H(S^2) - H(S^2 - 1)\}/\Gamma_2 \\
P(\tau_f) &= e^{-(\tau_f - \tau_0)^2/2\sigma_\tau^2} \cdot H(\tau_f)/\Gamma_3 \\
P(R_{ex}) &= 0.85\delta(R_{ex}) + 0.15 \cdot e^{-(R_{ex} - R_0)^2/2\sigma_R^2} \\
&\quad \cdot H(R_{ex})/\Gamma_4
\end{aligned}
$$

where Γ_i (i=1,...,4) normalizes the probability, H(x) is the Heaviside step function, $\delta(x)$ is the Dirac delta function, $S_0^2 = 0.85$, $\sigma_S = 0.15$, $\tau_0 = 0.025$ ns, $\sigma_{\tau o} = 0.025$ ns. R_{ex} values and the associated standard deviations were scaled to reflect the observed values in experimental data. As noted earlier, the ability to observe R_{ex} terms of a given size scales with the tumbling time (size of R_{ex} compared to R_2) and the experimental error (size of R_{ex} compared to the error in R_2). Therefore, the values of R_{ex} used in the synthetic data sets were set to $R_{ex0} = 1.5\ s^{-1}$ with $\sigma_{Rex} = 1.0\ s^{-1}$ for $\tau_c = 5.92$ ns, and $R_{ex0} = 2.5\ s^{-1}$ with $\sigma_{Rex} = 2.0\ s^{-1}$ for $\tau_c = 13.7$ ns. Large-amplitude internal motions on a time scale greater than a few hundred picoseconds (described using the extended model of Clore et al. (1990)) are not considered in the analysis of synthetic data for two reasons: first, because it has been shown that many such motions may be artifacts of an isotropic analysis of an anisotropic diffusor or transient dimer (Schurr et al., 1994; Phan et al., 1996; Luginbuhl et al., 1997); second, because it is assumed that residues undergoing large-amplitude internal motions can be identified through low heteronuclear NOE values (filter step 1a) (Tjandra et al., 1995; de Alba et al., 1999), through reduced T_1 and T_2 values (filter step 1b), through large values of τ_f (filter step 2b), or through failure to fit the Lipari–Szabo model of internal motion (filter step 2b).

Values of T_1, T_2 and NOE were calculated from these parameters of global and internal motion, and analyzed by the same filtering and analysis process as applied to the experimental data. Two protein sizes were considered, small ($\tau_c = 5.92$ ns, with associated synthetic T_1, T_2 and NOE errors of 1.3%, 2.7%, and 4.0%, respectively) and large ($\tau_c = 13.7$ ns, with associated synthetic T_1, T_2 and NOE errors of 3.3%, 3.5%, and 7.7%, respectively). These synthetic errors, required for minimization of χ^2, were based on the average experimental errors of SH3 and OspA, respectively. The input values of the global and internal motions were not used to direct the filtering and analysis, but were compared at the end to determine the accuracy of the analysis.

Results and discussion

Efficacy of the filter demonstrated using synthetic data sets

The performance of the filters is assessed using only prolate diffusion tensors. For an oblate diffusion tensor and a spherical distribution of bond vectors, there will be a high population of residues with low T_2 values, since they will be close to 90° from the unique axis of the diffusion tensor. Hence, due to the redundancy of these residues, the estimate of anisotropic tumbling is

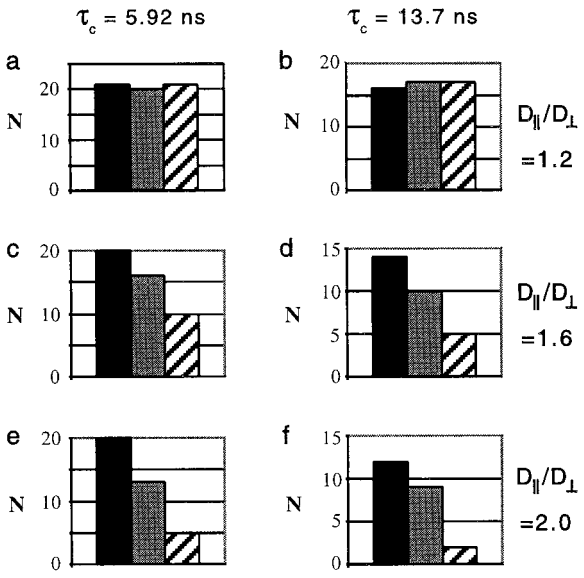

Figure 2. Number of residues (N) with $\alpha < 30°$ remaining after application of the coarse filter (gray) or the standard filter $(\langle T_2\rangle - T_{2,n})/\langle T_2\rangle - (\langle T_1\rangle - T_{1,n})/\langle T_1\rangle > 1.5 \times$ SD (hatched) (Tjandra et al., 1995), in comparison with the number of residues for which NOE > 0.65 and $R_{ex} < 1$ (black). The comparison is shown for two protein sizes, $\tau_c = 5.92$ ns (a,c,e), and $\tau_c = 13.7$ ns (b,d,f), and three different degrees of anisotropy, $D_\parallel/D_\perp = 1.2$ (a,b), $D_\parallel/D_\perp = 1.6$ (c,d), and $D_\parallel/D_\perp = 2.0$ (e,f). All values of $D_\parallel/D_\perp$ are greater than 1, since only prolate diffusion tensors were considered.

less likely to be skewed by exclusion of a few residues falsely identified as experiencing chemical exchange. Therefore, while a careful separation of global and internal motions is always important, it is much more important for the case of prolate diffusion tensors, which have a low population of residues with low T_2 values.

The following criteria are used to evaluate filter performance: retention of residues with large projections along the unique axis of the prolate diffusion tensor, removal of residues from the global tumbling data set that require three internal motion parameters, accuracy of the extracted parameters of global tumbling, and accuracy of the extracted parameters of internal motion. These comparisons demonstrate that the proposed filter shows increasing improvement over the standard filter with increasing anisotropy, and significant improvement for large anisotropy.

We first assessed the performance of the proposed coarse filter versus the standard filter by comparing the retention of residues with large projections along the unique axis of the diffusion tensor ($0 < \alpha_D \lesssim 30$) (Figure 2). These residues hold important information regarding anisotropic tumbling (Figure 1a,b), and their loss can skew the global tumbling analysis toward a more isotropic fit. The filters were applied to synthetic data sets for two protein sizes, $\tau_c = 5.92$ ns, and $\tau_c = 13.7$ ns, and for three different degrees of anisotropy, $D_\parallel/D_\perp = 1.2$, 1.6, and 2.0 (Figure 2). As shown in Figure 2, changes in the global tumbling time alter the number of residues with NOE < 0.65, as would be expected, but otherwise have little effect on the filter performance. For small anisotropy, the two filters retain approximately the same number of residues (Figure 2a,b). For intermediate anisotropy, the difference in retention between the two filters becomes noticeable, with the proposed filter retaining from 1.5–2 times as many of these critical residues (Figure 2c,d). For large anisotropy, the difference between the two filters is striking, with the proposed filter retaining from 2–4 times as many residues (Figure 2e,f). The underlying mechanism by which the standard filter rejects more residues aligned near the principal axis of the diffusion tensor is illustrated in Table 2. As can be seen from the table, as anisotropy increases, residues with small values of alpha (prolate ellipsoid) or large values of alpha (oblate ellipsoid) are increasingly likely to be cut (T_2 is lower and T_1 is higher than average). Residues with small contributions to chemical exchange are increasingly less likely to be cut.

The clear trends in the ability of each filter to retain residues with N-H bonds aligned near the principal axis of diffusion (Figure 2) imply that the filters will differ in their ability to accurately characterize global tumbling. We have chosen to demonstrate the correlation between retention of these residues and increased accuracy in determination of parameters of motion by examining the extreme cases of small anisotropy (similar retention, Figure 2a) and large anisotropy (dramatically different retention, Figure 2f). Hence, we continue our analysis of filter performance using synthetic SH3 ($\tau_c = 5.92$ ns, $D_\parallel/D_\perp = 1.22$) and synthetic OspA ($\tau_c = 13.7$ ns, $D_\parallel/D_\perp = 1.99$) as our test cases.

We next asked whether application of the proposed fine filter offered a significant improvement as compared to the coarse filter step alone. A successful application of the fine filter should have three results: (1) an improvement in the estimate of the anisotropy and global tumbling time; (2) continuing retention of residues with N-H bond vectors close to the principal axis of diffusion; (3) removal of residues that do not fit the Lipari–Szabo model for internal motion,

Table 2. Result of applying the standard filter in cases where T_1 and/or T_2 deviate from average

T_2	T_1	$\langle T_2\rangle - T_{2,i}/\langle T_2\rangle$	$\langle T_1\rangle - T_{1,i}/\langle T_1\rangle$	Result[c]	If $D_2 \sim D_1$	Probable outcome	Probable desired outcome
Lower	Lower	$+D_2$[a]	$+D_1$[b]	$D_2 - (+D_1)$	~ 0	Kept	Cut
Lower	Higher	$+D_2$	$-D_1$	$D_2 - (-D_1)$	$\sim +2\,D_2$	Cut	Kept
Higher	Lower	$-D_2$	$+D_1$	$-D_2 - (+D_1)$	$\sim -2\,D_2$	Kept	Kept
Higher	Higher	$-D_2$	$-D_1$	$-D_2 - (-D_1)$	~ 0	Kept	Cut
Lower	Average	$+D_2$	0	$D_2 - 0$	$\sim +D_2$	Cut or kept	Cut

[a] D_2 describes the fractional deviation of T_2 from average, as given by $\langle T_2\rangle - T_{2,i}/\langle T_2\rangle$.
[b] D_1 describes the fractional deviation of T_1 from average, as given by $\langle T_1\rangle - T_{1,i}/\langle T_1\rangle$.
[c] Result from applying the standard filter, where a residue is cut if $(\langle T_2\rangle - T_{2,i})/\langle T_2\rangle - (\langle T_1\rangle - T_{1,i})/\langle T_1\rangle > 1.5$ SD (SD is the standard deviation of the left-hand side of the equation).

to prevent underdetermined fits of the internal motion parameters. As shown in Table 3, the additional application of the fine filter corrects the overestimates of the anisotropy and of the tumbling time that remained after application of the coarse filter. In proceeding from the coarse filter to the fine filter, a retrospective analysis shows that the fine filter cut only those residues that should have been cut, due to the presence of R_{ex}. Hence, the retention of residues that strongly reflect anisotropic tumbling is maintained throughout the filtering process. By contrast, adding a fine filter step onto the standard filter is not expected to be particularly helpful in correctly determining the global tumbling of proteins with moderate to large anisotropy, since the residues that strongly reflect anisotropic tumbling have been irrevocably removed. The success of the total proposed filter (coarse + fine) in avoiding underdetermined fits is described below.

The performance of the total proposed filter and the standard filter in reproducing the global tumbling parameters was also compared (Table 3). For small anisotropy, the proposed filter comes closer to the synthetic values of $D_\parallel/D_\perp$ and θ, but the standard filter comes closer to the synthetic global tumbling time. For large anisotropy, the proposed filter better reproduces all of the synthetic tumbling parameters. In both cases, the standard filter underestimates the anisotropy as reflected by lower values of $D_\parallel/D_\perp$.

For measurements of T_1, T_2 and NOE at a single magnetic field strength, the ability of any filtering approach to eliminate residues that require more than two fitted internal motion parameters (S^2, τ_f) is important for avoiding underdetermined fits. Residues requiring three fitted parameters (S^2, τ_f, R_{ex}) are described here as non Lipari–Szabo. The proposed filter successfully identifies residues with $R_{ex} > 1\ s^{-1}$ as non Lipari–Szabo 100% of the time, for both large (27 out of 27) and small (22 out of 22) anisotropy. While the standard filter identifies 100% of these residues (22 out of 22) for small anisotropy, it fails to identify two residues with $R_{ex} > 1\ s^{-1}$ in the case of large anisotropy (25 out of 27). Therefore, the proposed filter successfully avoids underdetermined fits for both large and small anisotropy, while the standard filter has underdetermined fits for two residues in the case of large anisotropy.

Table 3. Comparison of the synthetic[a] and calculated[b] global tumbling parameters resulting from different filtering approaches

	$D_\perp$ (ns^{-1})	$D_\parallel$ (ns^{-1})	$D_\parallel/D_\perp$	τ_c (ns)	θ[c] (°)
OspA					
Synthetic[a]	0.00913	0.0182	1.99	13.7	0
Calculated[b]					
Proposed (coarse)	0.00891	0.0182	2.04	13.9	−2
Proposed (total)	0.00920	0.0183	1.99	13.6	0
Standard	0.00928	0.0174	1.88	13.9	−2
SH3					
Synthetic[a]	0.0262	0.0321	1.22	5.92	0
Calculated[b]					
Proposed (coarse)	0.0256	0.0321	1.25	6.00	−10
Proposed (total)	0.0264	0.0321	1.21	5.89	−1
Standard	0.0263	0.0316	1.20	5.93	−4

[a] The synthetic values of the global tumbling parameters are chosen as described in Materials and methods, and used to generate synthetic values of T_1, T_2, and NOE.
[b] Calculated values of the global tumbling parameters are obtained from the synthetic values of T_1, T_2 and NOE, that survived the indicated filtering process, as described in Materials and methods.
[c] θ is the angle between the unique axes of the inertia and diffusion tensors.

We then asked the question whether residues identified as non Lipari–Szabo could be satisfactorily fit using the chemical exchange model. If the data were fit perfectly, all non Lipari–Szabo residues in our synthetic data sets would fit the chemical exchange model, since the data were generated using either the Lipari–Szabo two-parameter (S^2, τ_f) model alone, or the three-parameter (S^2, τ_f, R_{ex}) model describing chemical exchange. For both filters, not all of the residues correctly identified as non Lipari–Szabo could be fit with the R_{ex} model. For small anisotropy, the proposed filter correctly identified 19 of the 22 non Lipari–Szabo residues as requiring R_{ex} terms, compared with 20 out of 22 for the standard filter. For large anisotropy the proposed filter correctly identified 21 of the 27 non Lipari–Szabo residues as requiring R_{ex} terms, compared with 15 out of 27 for the standard filter. This shows that both filters perform similarly in identification of R_{ex} for small anisotropy, while the proposed filter displays a significant improvement in this respect over the standard filter for large anisotropy. The failure to identify R_{ex} is largely due to the imperfect characterization of the global tumbling parameters. Hence, as expected from the design of the proposed filter, the successful distinction between R_{ex} and anisotropy in the filtering process results in more accurate modeling of anisotropic global tumbling, which in turn allows more accurate identification of residues significantly affected by chemical exchange.

As a final assessment, the accuracies of the proposed filter and the standard filter in reproducing the internal motion parameters for synthetic OspA and SH3 were compared (Table 4). As previously noted, an isotropic analysis of a protein undergoing anisotropic tumbling can lead to the false prediction of R_{ex}. Here, we are investigating the more subtle effects of underestimating the anisotropy. While we do not see a false prediction of R_{ex}, we do see changes in the values of S^2, τ_f, R_{ex} and χ^2 that reflect compensation for the inaccurate estimate of the anisotropy. Across the protein both filters successfully reproduce S^2, as demonstrated by the small average rmsd between the synthetic and modeled values across the protein. The accuracy is reduced, however, for those residues with synthetic R_{ex}. The least accurate prediction of S^2 is for residues with synthetic R_{ex}, analyzed by the standard filter, in the case of large anisotropy. For small anisotropy, both filters successfully reproduce R_{ex} to within the size of the error in T_2. For large anisotropy, the accuracy of R_{ex} is not as good as for small anisotropy. For the new filter proposed here, the deviation of the R_{ex} values from their true values is slightly larger than the error in T_2. For the standard filter, the deviation of the R_{ex} values from their true values is more than twice the error in T_2. The largest difference in the accuracy of the two filters is in extraction of τ_f. For small anisotropy, both filters reproduce τ_f with a deviation of less than 10% from the true values. For large anisotropy, the standard filter produces values of τ_f with an overall average deviation from the true values of up to 40%. As noted above, this reflects compensation for the inaccurate estimate of the anisotropy, and has been noted by others (Luginbuhl et al., 1997).

In summary, the proposed filter shows increasing improvement over the standard filter with increasing anisotropy. The evaluation of the results of the proposed filtering method against the synthetic data shows that anisotropic tumbling parameters are reproduced to within 1% of their true values for both large and small anisotropy. In addition, for both large and small anisotropy, residues with $R_{ex} > 1$ are successfully identified 100% of the time, S^2 values are reproduced with extremely high accuracy, and τ_f and R_{ex} values are reproduced with accuracies on the order of the size of the errors in the synthetic data. This analysis provides confidence in using this approach for interpretation of the anisotropic tumbling and internal motion parameters obtained in the examination of experimental relaxation data.

It should be noted that cases such as partially folded proteins or proteins undergoing transient dimerization can contain pervasive ns or μs–ms timescale motions and present a special challenge. However, successive application of our proposed filter should approach the true global tumbling in the case of μs–ms motions, provided sufficient data is retained to characterize the diffusion tensor (Fushman et al., 2000). We suggest that if significant changes occur in the global tumbling parameters obtained from successive applications of the filtering process, this indicates that additional data (e.g. measurements at multiple field strengths) are required for accurate distinction between chemical exchange and anisotropic tumbling. In addition, as recently pointed out (Fushman et al., 2000), a minimal sampling of N-H bond vector orientations is necessary to accurately characterize the diffusion tensor. If the minimal sampling requirement is not met, then measurement of additional relaxation parameters (e.g. $^{13}C^{\alpha}$) will be necessary.

Table 4. Comparison of the accuracy of extracted internal motion parameters resulting from application of the total proposed filter and the standard filter

	Filter	S^2 rmsd[a]	% dev[b]	τ_f rmsd[a]	% dev[b]	R_{ex} rmsd[a]	% dev[b]
OspA							
All residues	proposed	0.001	0.1	0.001	3		
	standard	0.002	0.2	0.003	10		
Syn $R_{ex} > 1$ only	proposed	0.003	0.3	0.001	4	0.1	4
	standard	0.006	0.7	0.01	40	0.2	8
SH3							
All residues	proposed	0.001	0.1	0.001	4		
	standard	0.001	0.1	0.002	7		
Syn $R_{ex} > 1$ only	proposed	0.002	0.2	0.001	4	0.03	2
	standard	0.001	0.2	0.001	4	0.03	2

[a]The rmsd is the average pairwise deviation between the synthetic and calculated values of the parameters.
[b]The % dev is the average rmsd across the residues divided by the average value of the parameter across those residues.

Measured relaxation parameters for OspA strongly reflect anisotropy

Experimental ^{15}N T_1, $T_{1\rho}$, T_2 and NOE values obtained for OspA are shown in Figure 3. If an isotropic model for OspA global tumbling were assumed, the large variations in longitudinal and transverse relaxation times that appear in β-strands 5–13 might be interpreted as evidence for large variations in amplitudes of motion in this region. However, two pieces of evidence suggest that these variations are not due to large differences in amplitudes of motion, but rather to anisotropic tumbling. As previously reported, the crystal structure of OspA represents its predominant conformation in solution (Bu et al., 1998; Pham and Koide, 1998). Amide hydrogen exchange experiments revealed that the entire OspA molecule is highly stable on the time scale of seconds to days (Pham et al., 1998). The principal axes of the moment of inertia tensor estimated from the crystal structure are 1.0:0.90:0.21, indicative of a prolate ellipsoid. In addition, a comparison between the ^{15}N relaxation times and the angle between the N-H bond vectors and the unique axis of the moment of inertia tensor, α_I, shows a highly significant correlation. This correlation can be seen qualitatively in Figure 3, where values of α_I close to 0 correspond to high T_1 and low T_2 and $T_{1\rho}$ values, and values of α_I close to 90 correspond to low T_1 and high T_2 and $T_{1\rho}$ values. The correlation is most easily observed in β-strands 5–13, where the largest variations in α_I occur. The values of the linear correlation coefficients and the corresponding probabilities of the null hypothesis (Table 5) quantitatively confirm this correlation. Although the relationship between the relaxation parameters and α is not strictly linear, it is approximately linear between 0.25 and 1.25 radians (approximately 15°– 70°) (Figure 1a,b) and can be used to gain insight into the degree of anisotropic tumbling, as illustrated in Table 5.

^{15}N relaxation parameters for SH3 will be reported elsewhere (Wang, C. et al., unpublished results). Anisotropic tumbling is not as apparent in the raw data for SH3 as it is for OspA. The principal axes of the moment of inertia tensor for SH3, estimated from the X-ray crystal structure of nearly intact Src (Xu et al., 1999), are 1.0:0.93:0.70, and the correlation of the ^{15}N relaxation times with α_I is not statistically significant (Table 5). Nevertheless, evidence for the presence of anisotropic tumbling may be found by comparing the relative size of the T_1, T_2 and NOE correlations. This comparison is made after flexible residues (NOE < 0.65) are removed from the data set, since the relationship between relaxation times and global tumbling is best observed for relatively rigid N-H bonds. For an isotropically tumbling protein, none of the relaxation times should be correlated with α_I. Since the NOE is relatively independent of the global tumbling, it should remain largely uncorrelated with α_I in the case of anisotropic tumbling, while T_1 and T_2 will be more highly correlated. Table 5 shows the large difference in the correlation probabilities for T_1 and NOE of SH3 with α_I, indicating the possibility of anisotropic tumbling. When the diffusion tensor is known, the correlation of the ^{15}N relaxation times with α_D can be determined. The correlation of T_1 with α_D is significant ($P < 0.05$) (Taylor, 1982), and the correlation of $T_{1\rho}$ with α_D is highly significant, as shown

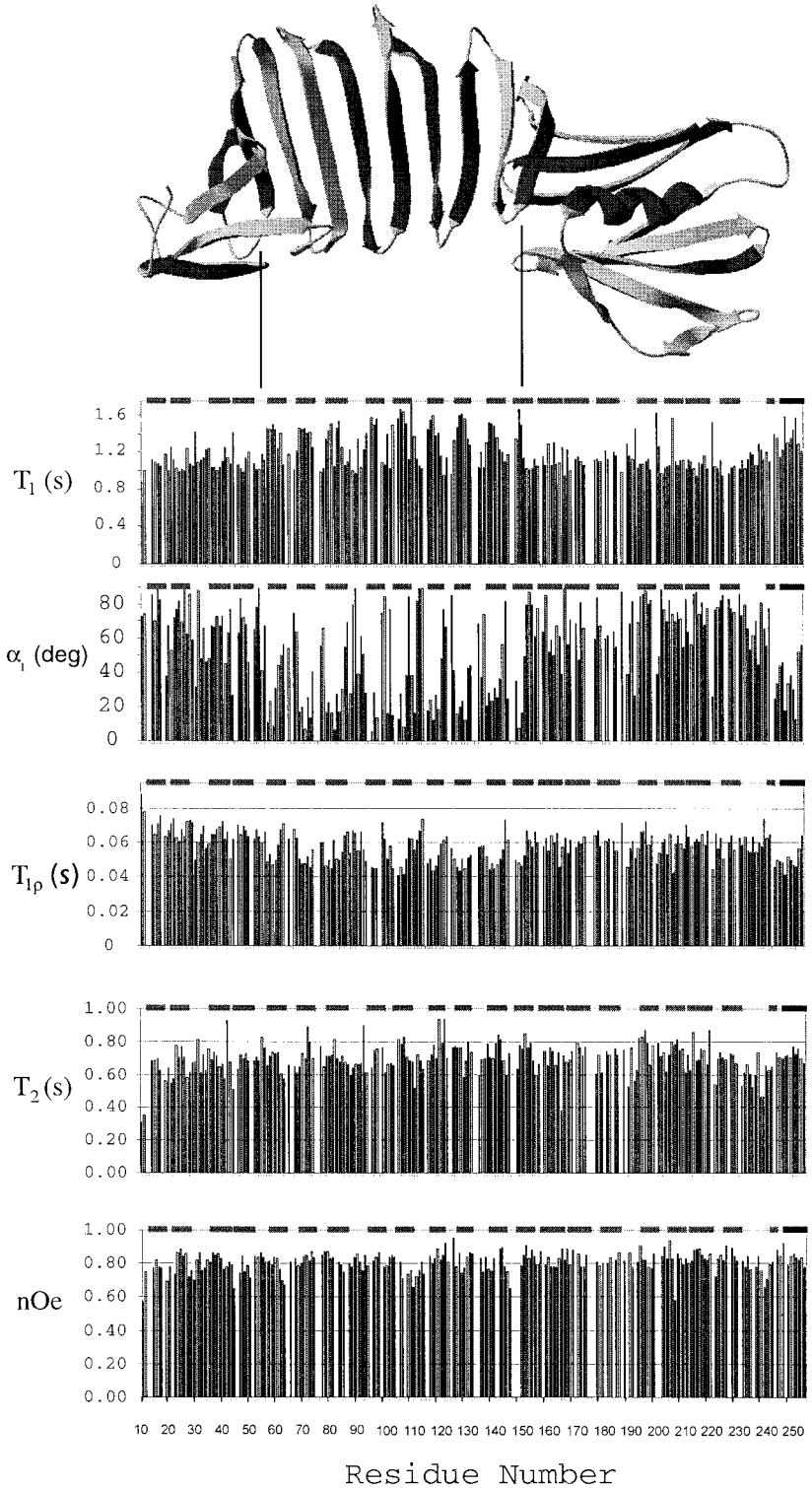

Figure 3. Experimental values of T_1, $T_{1\rho}$, T_2, NOE and α_I as a function of residue number for OspA. The ribbon diagram of OspA is shown at the top. Note that when α_I is close to 0, T_1 is higher than average and $T_{1\rho}$ is lower than average, while the NOE value is uncorrelated with α_I, as shown statistically in Table 5.

Table 5. Correlation of experimental ^{15}N relaxation data and S^2 values with N-H bond vector orientations for OspA and SH3

	T_1	T_2	NOE	S^2 (iso)	S^2 (aniso)
OspA (NOE > 0.65)					
Inertia r[a]	0.86	0.77	0.10	0.65	0.12
Inertia P[c]	3.3 E–28	6.2 E–23	0.20	4.0 E–15	0.12
SH3 (NOE > 0.65)		**$T1_\rho$**			
Inertia r[a]	0.38	0.26	0.19	0.27	0.085
Inertia P[c]	0.021	0.12	0.26	0.11	0.61
Diffusion r[b]	0.41	0.49	0.20	0.28	0.22
Diffusion P[c]	0.012	0.0028	0.22	0.098	0.18

[a]Linear correlation coefficient, r, between a given variable and α_I, where α_I is determined from the unique principal axis of inertia and defined between 0° and 90°.
[b]Linear correlation coefficient, r, between a given variable and α_D, where α_D is determined from the unique principal axis of diffusion and defined between 0° and 90°.
[c]The probability of the null hypothesis that the two variables are uncorrelated, as given by the complementary error function (Press et al., 1996). A small value of P indicates that the two distributions are significantly correlated. Values of P were calculated using 164 data points for OspA and 37 data points for SH3 in Mathematica™.

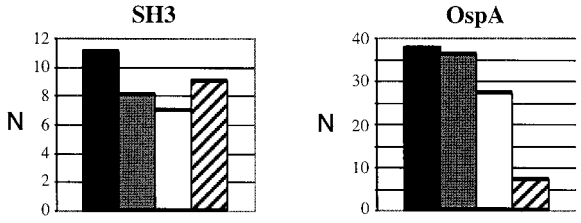

Figure 4. Application of filters to experimental data for SH3 (left) and OspA (right). The number of residues (N) with $\alpha < 30°$ remaining after application of the coarse filter (gray), total proposed filter (white), or standard filter (hatched), is shown in comparison with the number of residues remaining after the NOE filter alone (black).

in Table 5. When all of the evidence is considered, it is clear that anisotropic tumbling is the appropriate model for SH3, although its effects are much more subtle than those observed for OspA.

OspA and SH3 tumble as prolate ellipsoids

The proposed filter was applied to the measured relaxation data for OspA and SH3 to obtain the optimal global tumbling parameters. A comparison of the success of the proposed and standard filters in retaining residues with small values of α (Figure 4) shows that, as with synthetic data sets, differences between the two filters are more pronounced for large anisotropy. As will be reported elsewhere (Wang, C. et al., unpublished results), the global tumbling of SH3 is best described by a prolate ellipsoid. The optimized global tumbling parameters obtained here for OspA (Table 6) differ considerably from those obtained in a preliminary characterization (Pham and Koide, 1998). As expected, use of the standard filter in this preliminary characterization underestimated the anisotropy, yielding $D_\parallel/D_\perp = 1.75$. Here, using the total proposed filter, the reduced χ^2 value ($\chi^2_g/\upsilon = 1.4$, where υ is the number of degrees of freedom) and the F-test value ($F = 901$) clearly indicate that the relaxation is best described by an axially symmetric diffusion tensor, with $D_\parallel/D_\perp = 2.12$. As intuitively expected from the elongated shape of OspA, the unique principal axis of the diffusion tensor is oriented in the general direction of the long axis of the molecule (Figure 5). The unique axis of diffusion of SH3 is approximately aligned with the ligand-binding groove (Figure 5).

Additional confirmation that the contributions of global tumbling and internal motions to the ^{15}N relaxation times have been effectively separated comes from an examination of the correlation between values of S^2 and α, as shown in Table 5. An isotropic analysis of OspA yields a statistically significant correlation between S^2 and α (where α is measured relative to the unique axis of the moment of inertia tensor). Following the anisotropic analysis, this correlation is no longer significant, and is of the same order as the correlation of NOE with α. An isotropic analysis of SH3 yields a larger correlation between S^2 and α than be-

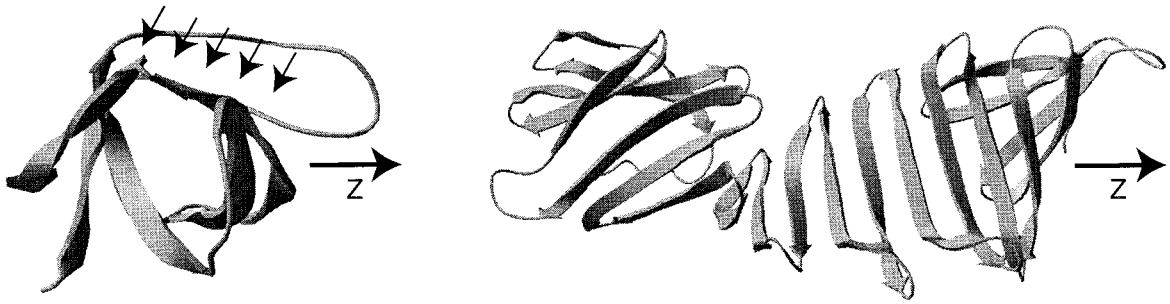

Figure 5. Ribbon diagrams of SH3 (left) and OspA (right) illustrating the relative orientation of each diffusion tensor. In each view the unique axis of the diffusion tensor (z) is oriented as shown. The SH3 ligand binding groove is indicated by a row of arrows.

Table 6. Global tumbling parameters for OspA using three different tumbling models. The axially symmetric anisotropic solution is statistically significant

Model	$\tau^{a}_{c,eff}$ (ns)	D_{xx} (ns^{-1})	D_{yy} (ns^{-1})	D_{zz} (ns^{-1})	θ $(^\circ)^b$	ϕ $(^\circ)^b$	ψ $(^\circ)^b$	χ^2_g/υ^c	F	P
Isotropic	15.0	0.0111	0.0111	0.0111	–	–	–	35.0	–	–
Axially symmetric	13.7	0.00887	0.00887	0.0188	175	148	–	1.40	901	9.8×10^{-77}
Asymmetric	13.7	0.00866	0.00917	0.0186	175	143	12	1.39	1.31	0.27

[a]At 45 °C, in water. $\tau_{c,eff}$ is calculated as $(1/2)(D_{xx}+D_{yy}+D_{zz})^{-1}$, where the D_{ii}'s are the magnitudes of the principal components of the diffusion tensor.
[b] The angles θ, ϕ, and ψ define the orientation of the diffusion tensor with respect to the moment of inertia frame of the X-ray crystallographic structure of OspA.
[c]113 residues were used to fit the final global tumbling parameters. Values of υ (number of degrees of freedom, i.e., number of data points – number of fitted parameters) are therefore 112, 109 and 107 for the isotropic, axially symmetric and fully anisotropic models, respectively.

tween NOE and α. Following the anisotropic analysis, the correlation between S^2 and α is reduced, and is of the same order as the correlation of NOE with α. This provides additional confirmation that the changes in longitudinal and transverse relaxation times due to global tumbling have been appropriately accounted for in both proteins.

Assessment of potential bias in T_2 measurements

The CPMG pulse train used in measurement of T_2 is more sensitive to slower ($\tau_{ex} > 30\,\mu s$) conformational exchange processes than the continuous wave (CW) pulse employed in measurement of $T_{1\rho}$, as shown in Figure 6. For this reason, T_2 measurements may be preferred over $T_{1\rho}$ for characterizing conformational exchange processes, particularly in large proteins. For large proteins such as OspA, R_{ex} is a smaller fraction of R_2, while the errors in R_2 are often larger, due to the smaller signal to noise ratio. However, as noted by others, numerous problems such as off-resonance effects can be associated with the CPMG pulse train (Lee and Wand, 1999). Therefore, to prevent potential bias introduced by systematic error associated with the CPMG pulse train, $T_{1\rho}$ values were also obtained for OspA, and $T1_\rho$ and T_2 measurements were compared. Residues for which $T1_\rho$ ($T'_{1\rho}$ corrected for off-resonance effects) (Akke and Palmer, 1996) and T_2 values differ by more than the sum of their errors can indicate either measurement error (random or systematic), or the presence of slow conformational exchange. In either case, the measured T_2 value can bias the global tumbling analysis. To reduce the impact of such bias, the estimated T_2 error (σ_{T2}) for OspA was increased for those residues for which $|T_{1\rho}-T_2|$ exceeded the sum of their errors, until the size of the sum of the errors was the same as the difference in the measured values. The filtering process and global tumbling analysis were then performed again. The changes in global tumbling resulting from this analysis, and an analysis in which these residues were completely removed from the data set are shown in Table 7. The minimal change in the global tumbling parameters suggests that, at least for OspA, the use of T_2 measurements did not significantly bias the global tumbling analysis.

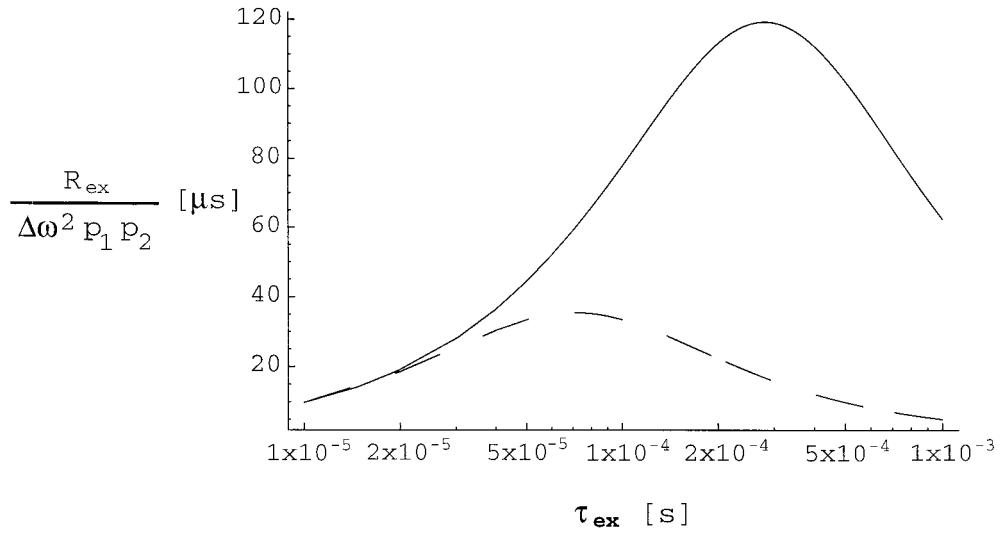

Figure 6. $R_{ex}/(p_1 p_2\ \Delta\omega^2)$ as a function of τ_{ex} for the CPMG (solid line) and CW (dashed line) experiments. Plots generated in Mathematica™ employing standard equations (Farrar and Becker, 1971), using $\omega_1 = 2243\ s^{-1}$, and $\tau_{cp} = 9 \times 10^{-4}$ s.

Table 7. Evaluation of potential bias in global tumbling parameters due to the use of T_2 versus $T_{1\rho}$ data for OspA.

	$D_{xx} = D_{yy}$	D_{zz}	θ (°)	φ (°)
Proposed filter	0.00886	0.0190	175	147
Proposed filter + $T_{1\rho}$ cut[a]	0.00884	0.0188	175	146
Proposed filter + $T_{1\rho}$ errs[b]	0.00887	0.0188	175	148

[a]In addition to those residues cut from the global tumbling data set by the proposed filter, all residues for which $T_{1\rho}$ and T_2 differed by more than the sum of the errors were removed.
[b]In addition to applying the proposed filter, for those residues with $T_{1\rho}$ and T_2 values differing by more than the sum of the errors, the size of the T_2 errors was increased, as described in the text.

Assessment of the effects of differences in N-H bond orientations between the OspA crystal and solution conformations

Since the X-ray crystal structure of OspA includes an additional Fab fragment bound to its N-terminal domain, the effects of possible discrepancies in α between the crystal and solution conformations were examined. To ensure that putative motions on the μs–ms time scale were not an artifact of differing domain orientations in the crystal and solution structures, the parameters of global tumbling and internal motion were optimized for the C-terminal domain alone (Skrynnikov et al., 2000). Optimizing the C-terminal region alone did not significantly affect the global tumbling parameters. In particular, the value of theta changed by only 2° (from 175° to 173°) when the C-terminal piece was considered separately. As would be expected, this modest change in orientation did not significantly change the number of residues requiring R_{ex} or the magnitude of the required R_{ex}. Of the residues subjected to the new round of optimization, 23 residues required R_{ex} before, and 20 residues required R_{ex} after. The average value of R_{ex} was 3 s^{-1} in both cases. We conclude, therefore, that the position of the domains as established by the crystal structure does not significantly differ from the average position observed in solution, and does not result in significant artifactual chemical exchange terms.

Conclusions

We have proposed a novel data filter for improving the distinction between chemical exchange and anisotropic tumbling in the analysis of ^{15}N relaxation parameters. This approach allows such distinction to be obtained with measurements of T_1, T_2 and NOE at a single magnetic field strength. Methods for identification and quantification of conformational exchange such as the use of multiple field strengths, rotating frame spin relaxation measurements, or cross-correlation measurements require significantly more experimental resources, such as additional spectrometer time and/or deuterium labeling. The method proposed here improves the accuracy of investigations of dynamics at a single field strength for proteins of known structure with significant anisotropic tumbling,

and allows an initial examination of μs–ms time scale motions.

The efficacy of the proposed filter is evaluated through comparison with a widely used data filter using both synthetic and experimental data sets. This evaluation demonstrates that the proposed filter accurately extracts the parameters describing global tumbling, with improved performance with increasing anisotropy as compared with the standard filter. The more accurate description of global tumbling allows a more accurate description of internal motions, including characterization of order parameters associated with ps–ns time scale motions. Changes in S^2 upon perturbation of the system (e.g. ligand binding) are increasingly being interpreted in terms of the corresponding change in entropy or free energy (Akke et al., 1993; Yang et al., 1997; Forman-Kay, 1999). However, changes in the state of a system, such as ligand binding, can change both the global tumbling and the internal motions, as recently shown for the SH3 domain of $pp60^{c-Src}$ (Wang, C. et al., unpublished results). As shown above, unless appropriately accounted for, the calculated values of S^2 will have an artifactual dependence on the global tumbling that could skew an entropic analysis. Hence, the proposed filter allows more accurate assessment of entropic contributions from the protein backbone to such processes as ligand binding.

Functionally relevant motions include flexibility on the μs–ms time scale (Palmer, A.G., et al., *Methods Enzymol.*, submitted). For example, the tips of the flaps that cover the active site of the HIV-1 protease undergo μs–ms time scale motions that may facilitate substrate access and product release (Nicholson et al., 1995). More recently, inhibitor binding to the protease was shown to increase motions on the millisecond time scale of the β-sheet dimer interface, motions that may enhance autoprocessing of the gag-pol polyprotein (Ishima et al., 1999). Millisecond time scale motions in the bacterial response regulator protein Spo0F have been shown to correlate with residues that are critical for protein–protein interactions with Spo0F signaling partners, implying that such motions play a role in selection of binding partners (Feher and Cavanagh, 1999). Hence, through minimizing artifacts in identification of residues experiencing chemical exchange, the proposed filtering approach will enable more accurate viewing of biologically relevant motions.

Acknowledgements

We thank Theresa A. Ramelot, Jason D. Gans and Dennis A. Torchia for valuable comments and discussion, Lewis E. Kay for use of his pulse sequence library, and Frank Delaglio and Dan Garrett (NIH/NIDDK) for use of their NMR software tools. This research was funded by the NSF (MCB-9808727), and NIH R01-GM57215 (S.K.). Fellowship stipend support for N.H.P. was provided by the National Physical Science Consortium and the Department of Energy through Lawrence Livermore National Laboratory.

References

Akke, M., Bruschweiler, R. and Palmer, A.G. (1993) *J. Am. Chem. Soc.*, **115**, 9832–9833.

Akke, M. and Palmer, A.G. (1996) *J. Am. Chem. Soc.*, **118**, 911–912.

Andrec, M., Montelione, G.T. and Levy, R.M. (1999) *J. Magn. Reson.*, **139**, 408–421.

Bevington, P.R. and Robinson, D.K. (1992) *Data Reduction and Error Analysis for the Physical Sciences*, McGraw-Hill, Boston, MA.

Bu, Z.M., Koide, S. and Engelman, D.M. (1998) *Protein Sci.*, **7**, 2681–2683.

Cavanagh, J., Fairbrother, W.J., Palmer, A.G. and Skelton, N.J. (1996) *Protein NMR Spectroscopy: Principles and Practice*, Academic Press, San Diego, CA.

Clore, G.M., Szabo, A., Bax, A., Kay, L.E., Driscoll, P.C. and Gronenborn, A.M. (1990) *J. Am. Chem. Soc.*, **112**, 4989–4991.

Cordier, F., Wang, C., Grzesiek, S. and Nicholson, L.K. (2000) *J. Mol. Biol.*, **304**, 497–505.

de Alba, E., Baber, J.L. and Tjandra, N. (1999) *J. Am. Chem. Soc.*, **121**, 4282–4283.

Farrar, T.C. and Becker, E.D. (1971) *Pulse and Fourier Transform NMR: Introduction to Theory and Methods*, Academic Press, New York, NY.

Farrow, N.A., Muhandiram, R., Singer, A.U., Pascal, S.M., Kay, C.M., Gish, G., Shoelson, S.E., Pawson, T., Forman-Kay, J.D. and Kay, L.E. (1994) *Biochemistry*, **33**, 5984–6003.

Feher, V.A. and Cavanagh, J. (1999) *Nature*, **400**, 289–293.

Forman-Kay, J.D. (1999) *Nat. Struct. Biol.*, **6**, 1086–1087.

Fushman, D., Ghose, R. and Cowburn, D. (2000) *J. Am. Chem. Soc.*, **122**, 10640–10649.

Grzesiek, S. and Bax, A. (1993) *J. Am. Chem. Soc.*, **115**, 12593–12594.

Ishima, R., Freedberg, D.I., Wang, Y.X., Louis, J.M. and Torchia, D.A. (1999) *Struct. Fold. Des.*, **7**, 1047–1055.

Jia, X., Lee, L.K., Light, J., Palmer, A.G. and Assa-Munt, N. (1999) *J. Mol. Biol.*, **292**, 1083–1093.

Kay, L.E., Torchia, D.A. and Bax, A. (1989) *Biochemistry*, **28**, 8972–8979.

Kroenke, C.D., Loria, J.P., Lee, L.K., Rance, M. and Palmer, A.G. (1998) *J. Am. Chem. Soc.*, **120**, 7905–7915.

Lee, A.L. and Wand, A.J. (1999) *J. Biomol. NMR*, **13**, 101–112.

Lee, L.K., Rance, M., Chazin, W.J. and Palmer, A.G. (1997) *J. Biomol. NMR*, **9**, 287–298.

Li, H., Dunn, J.J., Luft, B.J. and Lawson, C.L. (1997) *Proc. Natl. Acad. Sci. USA*, **94**, 3584–3589.

Lipari, G. and Szabo, A. (1982) *J. Am. Chem. Soc.*, **104**, 4546–4559.

Luginbuhl, P., Pervushin, K.V., Iwai, H. and Wüthrich, K. (1997) *Biochemistry*, **36**, 7305–7312.

Mandel, A.M., Akke, M. and Palmer, A.G. (1995) *J. Mol. Biol.*, **246**, 144–163.

Nicholson, L.K., Kay, L.E., Baldisseri, D.M., Arango, J., Young, P.E., Bax, A. and Torchia, D.A. (1992) *Biochemistry*, **31**, 5253–5263.

Nicholson, L.K., Yamazaki, T., Torchia, D.A., Grzesiek, S., Bax, A., Stahl, S.J., Kaufman, J.D., Wingfield, P.T., Lam, P.Y.S., Jadhav, P.K., Hodge, C.N., Domaille, P.J. and Chang, C.H. (1995) *Nat. Struct. Biol.*, **2**, 274–280.

Palmer, A.G., Wright, P.E. and Rance, M. (1991) *Chem. Phys. Lett.*, **185**, 41–46.

Pham, T.N., Koide, A. and Koide, S. (1998) *Nat. Struct. Biol.*, **5**, 115–119.

Pham, T.N. and Koide, S. (1998) *J. Biomol. NMR*, **11**, 407–414.

Phan, I.Q.H., Boyd, J. and Campbell, I.D. (1996) *J. Biomol. NMR*, **8**, 369–378.

Press, W.H., Teukolsky, S.A., Vetterling, W.T. and Flannery, B.P. (1996) *Numerical Recipes in C: The Art of Scientific Computing*, Press Syndicate of the University of Cambridge, New York, NY.

Raiford, D.S., Fisk, C.L. and Becker, E.D. (1979) *Anal. Chem.*, **51**, 2050–2051.

Schurr, J.M., Babcock, H.P. and Fujimoto, B.S. (1994) *J. Magn. Reson.*, **B105**, 211–224.

Skrynnikov, N.R., Goto, N.K., Yang, D.W., Choy, W.Y., Tolman, J.R., Mueller, G.A. and Kay, L.E. (2000) *J. Mol. Biol.*, **295**, 1265–1273.

Taylor, J.R. (1982) *An Introduction to Error Analysis: The Study of Uncertainties in Physical Measurements*, Oxford University Press, Mill Valley, CA.

Tjandra, N., Feller, S.E., Pastor, R.W. and Bax, A. (1995) *J. Am. Chem. Soc.*, **117**, 12562–12566.

Tjandra, N., Wingfield, P., Stahl, S. and Bax, A. (1996) *J. Biomol. NMR*, **8**, 273–284.

Woessner, D.E. (1962) *J. Chem. Phys.*, **37**, 647–654.

Xu, W., Doshi, A., Lei, M., Eck, M.J. and Harrison, S.C. (1999) *Mol. Cell*, **3**, 629–638.

Yamazaki, T., Muhandiram, R. and Kay, L.E. (1994) *J. Am. Chem. Soc.*, **116**, 8266–8278.

Yang, D.W., Mok, Y.K., Forman-Kay, J.D., Farrow, N.A. and Kay, L.E. (1997) *J. Mol. Biol.*, **272**, 790–804.